

Topological semimetal phase with exceptional points in 1D non-Hermitian systems

Kazuki Yokomizo¹ and Shuichi Murakami^{1,2}

¹*Department of Physics, Tokyo Institute of Technology,
2-12-1 Ookayama, Meguro-ku, Tokyo, 152-8551, Japan*

²*TIES, Tokyo Institute of Technology, 2-12-1 Ookayama, Meguro-ku, Tokyo, 152-8551, Japan*

To describe eigenstates in non-Hermitian crystalline systems, the non-Bloch band theory has recently been established, and the generalized Brillouin zone (GBZ) has unique features which are absent in Hermitian systems. In this Letter, we show that in one-dimensional non-Hermitian systems with both sublattice symmetry and time-reversal symmetry, a topological semimetal phase with exceptional points is stable. This stems from the unique features of the GBZ. We can relate the motion of the exceptional points with the change of the value of a topological invariant characterizing a topological insulator phase. It is also shown that the energy bands are divided into three region, depending on the symmetry of the eigenstates.

Non-Hermitian quantum mechanics has been attracting much attention in many fields of physics in the past decades. Many experimental studies have realized various physical systems with non-Hermitian effects¹⁻¹⁹. Among these experimental studies, appearance of exceptional points and rings where some energy eigenvalues become degenerate and the corresponding eigenstates coalesce^{20,21}, and intriguing phenomena have been observed²²⁻³³. At such non-Hermitian degeneracy, since the Hamiltonian is non-diagonalizable, these degeneracies are unique to non-Hermitian systems. As is motivated by these experimental studies, existence of exceptional points, rings, and surfaces, and phenomena induced by them have been theoretically predicted in various physical systems³⁴⁻⁶¹, and under some symmetries, they are classified in terms of topology⁶²⁻⁶⁶.

Recent theoretical studies have been focusing on topological systems in solid state physics⁶⁷⁻⁷⁹. The bulk-edge correspondence has been notably under debate⁸⁰⁻¹¹⁰ since it seems to be violated in contrast to Hermitian systems. The main issue of the bulk-edge correspondence in non-Hermitian systems is that there is a difference between the energy spectrum in a periodic chain and that in an open chain. This difference is caused by the non-Hermitian skin effect⁸³. In Refs. 83 and 102, it was shown that while the Bloch wave number k takes a real value in a periodic chain, it becomes complex in an open chain, and that the value of $\beta \equiv e^{ik}$ is confined on a loop on the complex plane so that continuum bands are reproduced in a large open chain. Then the loop of β is called the generalized Brillouin zone (GBZ) C_β , which is a generalization of the Brillouin zone in Hermitian systems. We note that C_β is deformed as the system parameters change and that it can have cusps¹⁰². As a result, one can establish bulk-edge correspondence between the topological invariant defined in terms of C_β and existence of the topological edge states in some cases.

In this Letter, we show that the non-Hermitian modification of the GBZ C_β gives qualitative changes to physics of topological semimetals (TSMs). Because of this modification, the TSM phase with exceptional points is stable in one-dimensional (1D) non-Hermitian systems. The

phase is topologically protected by both sublattice symmetry (SLS) and time-reversal symmetry (TRS), and therefore, it disappears if either the SLS or the TRS is broken. As system parameters change continuously, C_β is deformed so that gapless points always lie on C_β , and the system remains in the TSM phase. This TSM phase can be regarded as an intermediate phase between a normal insulator (NI) phase and a topological insulator (TI) phase characterized by a topological invariant. Then the creation and annihilation of the exceptional points can be related to the change of this topological invariant. We also find that the continuum bands are divided into three regions, where the energies become real, pure imaginary, and complex, depending on the symmetry of the eigenstates.

For illustration of the stabilization of the TSM phase, in Fig. 1, we show an evolution of our model, whose details are explained later, upon a change of a system parameter μ . In Fig. 1(c-1)-(h-1), a gap in the system closes if the GBZ C_β goes through one of gap-closing points represented by the red or blue dots and squares. In particular, one can see from Figs. 1(e-1) and (f-1) that as μ changes, C_β is deformed so that it keeps the gap closed. We also find that the phase transitions between the NI and TI phases are qualitatively different from Hermitian systems. For example, in Fig. 3(b), at the phase transition, the exceptional points come to the cusps, and in total, the gap closes at three points on C_β . These novel behaviors never occur when the Bloch wave number takes real values. Since in such a case, the Brillouin zone becomes a unit circle regardless of the values of the system parameters, the Brillouin zone cannot hold the gap-closing point (Figs. 2(c) and (d)), and the gap closes only at isolated points along the μ -axis (Figs. 2(b) and (e)).

In the following, we study a 1D non-Hermitian tight-binding system with both the SLS and the TRS. For a real-space Hamiltonian H , these symmetries are defined as $\Gamma H \Gamma^{-1} = -H$, $\mathcal{T} H^* \mathcal{T}^{-1} = H$, where Γ and \mathcal{T} are unitary matrices. Here, due to the SLS, one can write

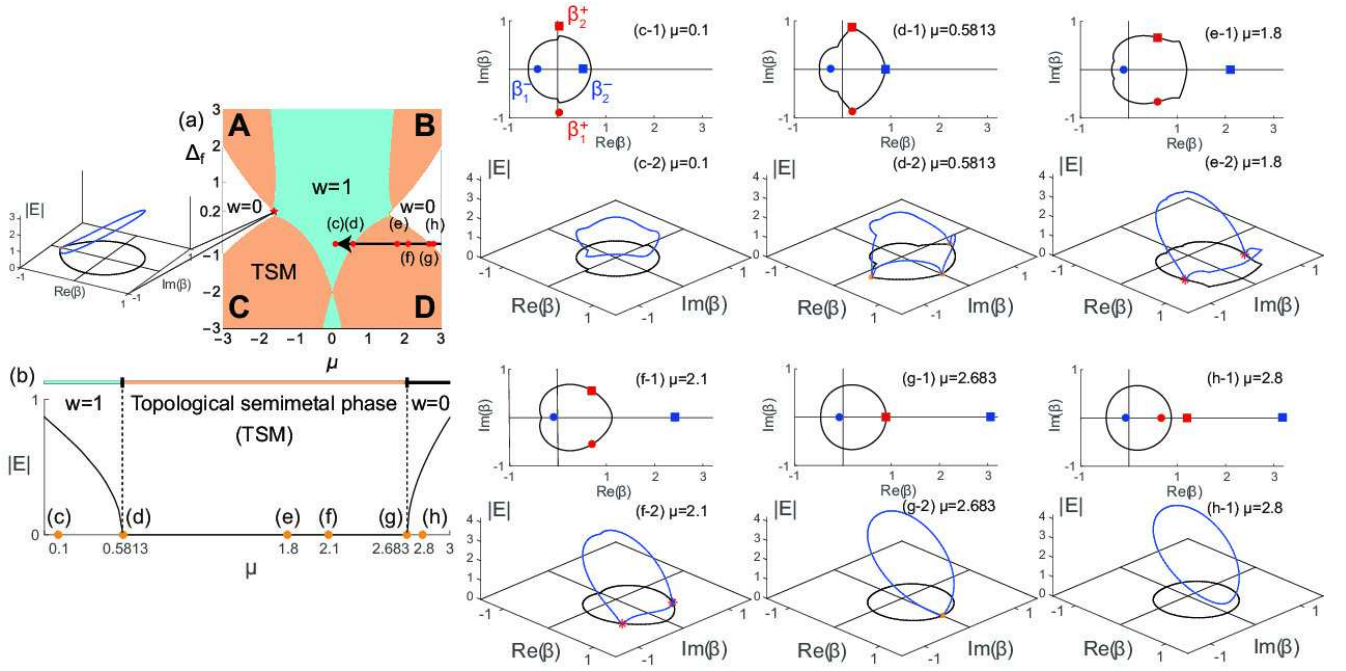


FIG. 1. (a) Phase diagram in the non-Hermitian Kitaev chain with $k \in \mathbb{C}$ with the values of the parameters to be $t_b = 1.2$, $t_f = 0.5$, $\Delta_b = 0.3$. At the red star ($\mu = -1.5922$ and $\Delta_f = 0.2$), the gap closes, and a direct transition between two insulator phases with $w = 0$ (white region) and $w = 1$ (blue region) occurs. The orange regions express the topological semimetal (TSM) phase. (b) Continuum band along the black arrow ($\Delta_f = -0.7$) in (a). Since it is a two-band model with the sublattice symmetry, we only show $|E|$ to see whether the gap closes. (c)-(h) Gap-closing points, generalized Brillouin zone, and motion of the exceptional points along the black arrow in (a). The red (or blue) dots and squares express the gap-closing points of the equation $R_+(\beta) = 0$ (or $R_-(\beta) = 0$).

the Bloch Hamiltonian $\mathcal{H}(\beta)$ with $2N$ bands as

$$\mathcal{H}(\beta) = \begin{pmatrix} 0 & R_+(\beta) \\ R_-(\beta) & 0 \end{pmatrix}, \quad (1)$$

where $R_{\pm}(\beta)$ are $N \times N$ matrices. Then the eigenvalue equation $\det[\mathcal{H}(\beta) - E] = 0$ yields the bands symmetric with respect to $E = 0$.

Next we mention the main point of the non-Bloch band theory in Ref. 102. In non-Hermitian systems, the Bloch wave number k becomes complex so that it describes continuum bands in a long open chain. The set of k forms the GBZ C_{β} . We note that the eigenvalue equation $\det[\mathcal{H}(\beta) - E] = 0$ is an algebraic equation for β with an even degree $2M$ in general, and we number the $2M$ solutions of $\det[\mathcal{H}(\beta) - E] = 0$ so as to satisfy $|\beta_1| \leq \dots \leq |\beta_{2M}|$. Then the condition for continuum bands is given by

$$|\beta_M| = |\beta_{M+1}|, \quad (2)$$

and the trajectories of β_M and β_{M+1} give C_{β} .

Now we describe the reason why the TSM phase is stable under the SLS and TRS. From the Bloch Hamiltonian (1), a condition for a gap closing at $E = 0$ is decomposed into two equations $\det R_+(\beta) = 0$ and $\det R_-(\beta) = 0$. Thanks to the TRS, $\det R_{\pm}(\beta)$ are polynomials of β and β^{-1} with real coefficients, and therefore, it follows that

any complex solutions of $\det R_{\pm}(\beta) = 0$ appear in complex conjugate pairs (β, β^*) . Then, if we suppose β_M and β_{M+1} form a pair of the complex conjugate solutions of $\det R_+(\beta) = 0$, they satisfy Eq. (2), meaning that β_M and β_{M+1} are on the GBZ, and the gap is zero. Even when system parameters change, the gap remains zero as long as this pair gives M th and $(M+1)$ th largest absolute values among the $2M$ solutions. In conclusion, the gapless region in the non-Hermitian system with the SLS and the TRS is robust against the change of system parameters.

To study how the TSM phase appears, we investigate the non-Hermitian Kitaev chain, which has been studied in some previous works^{104,111–119}. Its real-space Hamiltonian is written as

$$H = \sum_n \left[t_b c_n^\dagger c_{n+1} + t_f c_{n+1}^\dagger c_n - i\Delta_b c_n^\dagger c_{n+1}^\dagger - i\Delta_b^* c_n c_{n+1} + i\Delta_f c_{n+1}^\dagger c_n^\dagger + i\Delta_f^* c_{n+1} c_n - \mu c_n^\dagger c_n \right]. \quad (3)$$

This Hamiltonian reduces to that of the conventional Kitaev chain¹²⁰ when $t_b = t_f \equiv t \in \mathbb{R}$ and $\Delta_b = \Delta_f \equiv \Delta \in \mathbb{C}$.

We assume that the real-space Hamiltonian (3) satisfies both the SLS and the TRS, which sets all the parameters to be real. Then the Bloch Hamiltonian $\mathcal{H}(\beta)$ is expressed as the off-diagonal form (1) with

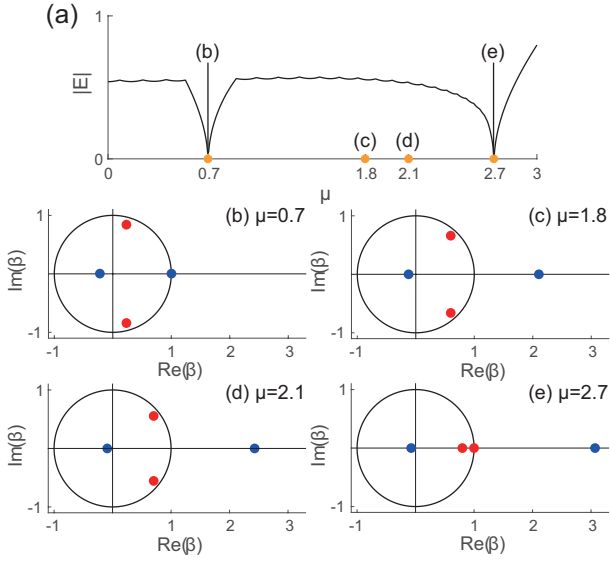


FIG. 2. (a) Continuum band and (b)-(e) Brillouin zone in the non-Hermitian Kitaev chain with $k \in \mathbb{R}$. The red (or blue) dots express the gap-closing points of the equation $R_+(\beta) = 0$ (or $R_-(\beta) = 0$). The values of parameters are $t_b = 1.2$, $t_f = 0.5$, $\Delta_b = 0.3$, and $\Delta_f = -0.7$.

$R_{\pm}(\beta) = (t_b \pm \Delta_b)\beta - \mu + (t_f \mp \Delta_f)\beta^{-1}$, where $\beta \equiv e^{ik}$, $k \in \mathbb{C}$. The eigenvalue equation is written as $\det[\mathcal{H}(\beta) - E] = E^2 - R_+(\beta)R_-(\beta) = 0$. Since it is a quartic equation for β , the condition for continuum bands can be written as $|\beta_2| = |\beta_3|$ when the solutions satisfy $|\beta_1| \leq |\beta_2| \leq |\beta_3| \leq |\beta_4|$ ¹⁰². We note that the GBZ is always a single loop encircling the origin on the complex plane^{106,121}.

The insulator phases of this system are classified in terms of a Z topological invariant called winding number w because it has the SLS, defined as¹⁰²

$$w = -\frac{w_+ - w_-}{2}, \quad w_{\pm} = \frac{1}{2\pi} [\arg R_{\pm}(\beta)]_{C_{\beta}}, \quad (4)$$

where $[\arg R_{\pm}(\beta)]_{C_{\beta}}$ means the change of the phase of the functions $R_{\pm}(\beta)$ as β goes along the GBZ C_{β} in a counterclockwise way. As long as there is a gap at $E = 0$, $R_{\pm}(\beta)$ never vanish along C_{β} , and w is well defined.

Figure 1(a) shows the phase diagram of our model, with the NI phase with $w = 0$ (white region), the TI phase with $w = 1$ (blue region), and the TSM phase (orange region). In the TSM phase, the gap closes at $E = 0$, which means that the equation $R_+(\beta) = 0$ or $R_-(\beta) = 0$ holds somewhere on the GBZ C_{β} . At such a point on C_{β} , the Hamiltonian cannot be diagonalizable, and such point is called exceptional point. In other words, the orange region represents that the system has the exceptional points. We note that the TSM phase appears as an intermediate phase between the NI and TI phases.

Now we explain the mechanism of the appearance of this TSM phase. In our model, the solutions of the equa-

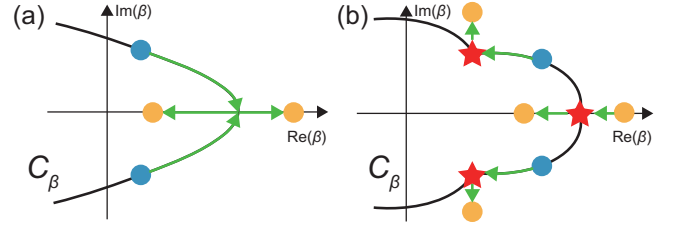


FIG. 3. Schematic figure of (a) coalescence of the exceptional points and (b) annihilation of the exceptional point at the cusp, respectively. The yellow (or blue) dots express the gap-closing points (or the exceptional points), and the red stars are the cusps.

tions $R_{\pm}(\beta) = 0$ are gap-closing points, shown as the red and blue dots and squares in Figs. 1(c-1)-(h-1), and they become the exceptional points when the GBZ C_{β} goes through them. Let $\beta = \beta_i^a$ ($i = 1, 2$, $a = +, -$) denote the gap-closing points of $R_a(\beta) = 0$, with $|\beta_1^a| \leq |\beta_2^a|$. In the regions A and B in Fig. 1(a), $R_-(\beta) = 0$ has two complex-conjugate gap-closing points, satisfying $\beta_1^- = (\beta_2^-)^*$, and their common absolute value $|\beta_1^-| = |\beta_2^-|$ is between the values of $|\beta_1^+|$ and $|\beta_2^+|$: $|\beta_1^+| \leq |\beta_1^-| = |\beta_2^-| \leq |\beta_2^+|$. Thus the condition (2) is satisfied, and therefore, β_1^- and β_2^- are on C_{β} and are the exceptional points. The condition $\beta_1^- = (\beta_2^-)^*$ remains satisfied even when the system parameter changes because $R_-(\beta) = 0$ is an algebraic equation with real coefficients. Thus the exceptional points move along C_{β} as shown in Figs. 1(c-2)-(h-2), and the system remains in the TSM phase. In the region C and D in Fig. 1(a), a similar scenario holds true, by exchanging $R_+(\beta)$ and $R_-(\beta)$.

Because of this mechanism for the stabilization of the exceptional points, annihilations (and likewise creations) of them are limited to two patterns as shown in Figs. 3(a) and (b). Figure 3(a) represents a coalescence of two exceptional points, and Fig. 3 (b) represents an encounter between the gap-closing point and the cusp. In Fig. 3(a), the two exceptional points meet and become two real gap-closing points. It occurs on the real axis. This can be seen in Fig. 1(g). On the other hand, the case of Fig. 3(b) occurs when two complex-conjugate exceptional points and one gap-closing point share the same absolute value. Therefore the gap closes at three points on the GBZ, for example, as shown in Fig. 1(d). At this point, $|\beta_1^-| = |\beta_2^-| = |\beta_2^+|$ is satisfied, and the ordering of the absolute values of three gap-closing points $\beta_{1,2}^-$ and β_2^+ change, allowing the exceptional point to disappear and the gap to open.

We can relate the creation and annihilation of the exceptional points with the change of the value of the winding number w defined in Eq. (4). For example, through the motion of the exceptional points as shown in Figs.1(c-1)-(h-1), we find that the number of the gap-closing points inside the GBZ is changed. Then, from Eq. (4), this motion changes the values of w_+ and w_- by

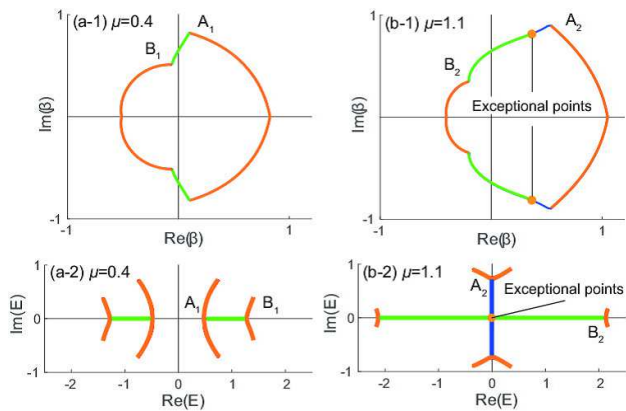


FIG. 4. Generalized Brillouin zone and continuum bands in the non-Hermitian Kitaev chain. TRS-unbroken region, STS-unbroken region, and TRS/STS-broken region are shown in green, in blue, and in orange, respectively. The values of the parameters are $t_b = 1.2$, $t_f = 0.5$, $\Delta_b = 0.3$, $\Delta_f = -0.7$, with (a) $\mu = 0.4$ and (b) $\mu = 1.1$.

1 and -1 , respectively, resulting in the change of w by 1. We show the detail of the argument in the Supplemental Material¹²².

Finally we show that in non-Hermitian systems with the SLS and TRS, the continuum bands are divided into three regions in terms of the symmetry of the eigenstates. In the first one, the energies are real, and eigenenergies of a time-reversal pair ($|\psi\rangle, \mathcal{T}|\psi\rangle^*$) are degenerate, i.e., $E = E^*$, where $|\psi\rangle$ is an eigenstate of the Hamiltonian. In the second region, the energies are pure imaginary, and a pair of states $|\psi\rangle$ and $\Gamma\mathcal{T}|\psi\rangle^*$ related by the sublattice-time-reversal symmetry (STS) is degenerate, i.e., $E = -E^*$. In the third region, the energies are complex, and neither the time-reversal pair nor the sublattice-time-reversal pair is degenerate. We call these three regions TRS-unbroken region, STS-unbroken region, and TRS/STS-broken region, respectively. For example, in the non-Hermitian Kitaev chain, we show the above three regions (Figs. 4(a-2)-(b-2)).

Importantly, these regions are connected to each other at the cusps or the exceptional points. In Fig.4(a-2) and (b-2), three curves meet at one point, where the GBZ C_β

have cusps represented by A_1 and B_1 (or A_2 and B_2). It is consistent with the property of the cusp, where three points on C_β share the same energy. Furthermore, in Fig. 4(b), the green and blue lines are connected at the exceptional point with $E = 0$. Thus the exceptional point connecting the real and pure-imaginary energies becomes stable because such structure is topologically protected by the symmetries.

In summary, we show that in 1D non-Hermitian systems with both the SLS and the TRS, the TSM phase with exceptional points is stable, unlike Hermitian systems. The appearance of the TSM phase is attributed to the unique features of the GBZ. It is shown that this TSM phase can be regarded as an intermediate phase between the NI and TI phases. We also find that the continuum bands are divided into three regions in terms of the symmetry of the eigenstates, and the regions change only at the cusps and the exceptional points. Thus non-Hermiticity brings about qualitative changes to the topological phase transition.

So far, we have treated the parameters Δ_b and Δ_f as real. When $\Delta_b, \Delta_f \in \mathbb{C}$, both the SLS and the TRS are broken. In this case, this system has only pseudo particle-hole symmetry (PHS)¹¹⁰. We show that the non-Hermitian systems with the pseudo PHS is classified in terms of a Z_2 topological invariant, and importantly, we find that the pseudo PHS cannot stabilize the TSM phase with exceptional points. We show some analyses in the Supplemental Material¹²².

We note that whether such TSM phase appears or not depends on symmetries of systems. When the systems have either chiral symmetry, pseudo TRS, or PHS¹¹⁰, the Bloch wave number becomes real, independent of any boundary conditions^{101,122}. Therefore the TSM phase cannot stably exist under either of these symmetries.

We are grateful for Ryo Okugawa and Ryo Takahashi for valuable discussions. This work was supported by JP18H03678 and JSPS KAKENHI Grant Numbers JP16J07354; by JST, CREST (No. JP-MJCR14F1); and by the MEXT Elements Strategy Initiative to Form Core Research Center (TIES). K. Y. was also supported by JSPS KAKENHI (Grant No. 18J22113).

¹ T. Eichelkraut, R. Heilmann, S. Weimann, S. Stützer, F. Dreisow, D. Christodoulides, S. Nolte, and A. Szameit, *Nat. Commun.* **4**, 2533 (2013).

² C. Poli, M. Bellec, U. Kuhl, F. Mortessagne, and H. Schomerus, *Nat. Commun.* **6**, 6710 (2015).

³ J. M. Zeuner, M. C. Rechtsman, Y. Plotnik, Y. Lumer, S. Nolte, M. S. Rudner, M. Segev, and A. Szameit, *Phys. Rev. Lett.* **115**, 040402 (2015).

⁴ Y.-L. Xu, W. S. Fegadolli, L. Gan, M.-H. Lu, X.-P. Liu, Z.-Y. Li, A. Scherer, and Y.-F. Chen, *Nat. Commun.* **7**, 11319 (2016).

⁵ S. Weimann, M. Kremer, Y. Plotnik, Y. Lumer, S. Nolte,

K. Makris, M. Segev, M. Rechtsman, and A. Szameit, *Nat. Mater.* **16**, 433 (2017).

⁶ L. Xiao, X. Zhan, Z. Bian, K. Wang, X. Zhang, X. Wang, J. Li, K. Mochizuki, D. Kim, N. Kawakami, *et al.*, *Nat. Phys.* **13**, 1117 (2017).

⁷ P. St-Jean, V. Goblot, E. Galopin, A. Lemaître, T. Ozawa, L. Le Gratiet, I. Sagnes, J. Bloch, and A. Amo, *Nat. Photonics* **11**, 651 (2017).

⁸ B. Bahari, A. Ndao, F. Vallini, A. El Amili, Y. Fainman, and B. Kanté, *Science* **358**, 636 (2017).

⁹ M. Parto, S. Wittek, H. Hodaei, G. Harari, M. A. Bandres, J. Ren, M. C. Rechtsman, M. Segev,

- D. N. Christodoulides, and M. Khajavikhan, *Phys. Rev. Lett.* **120**, 113901 (2018).
- ¹⁰ M. A. Bandres, S. Wittek, G. Harari, M. Parto, J. Ren, M. Segev, D. N. Christodoulides, and M. Khajavikhan, *Science* (2018), 10.1126/science.aar4005.
- ¹¹ M. Pan, H. Zhao, P. Miao, S. Longhi, and L. Feng, *Nat. Commun.* **9**, 1308 (2018).
- ¹² E. I. Rosenthal, N. K. Ehrlich, M. S. Rudner, A. P. Higginbotham, and K. W. Lehnert, *Phys. Rev. B* **97**, 220301(R) (2018).
- ¹³ J. Li, A. K. Harter, J. Liu, L. de Melo, Y. N. Joglekar, and L. Luo, *Nat. Commun.* **10**, 855 (2019).
- ¹⁴ M. Kremer, T. Biesenthal, L. J. Maczewsky, M. Heinrich, R. Thomale, and A. Szameit, *Nat. Commun.* **10**, 435 (2019).
- ¹⁵ Y. Wu, W. Liu, J. Geng, X. Song, X. Ye, C.-K. Duan, X. Rong, and J. Du, *Science* **364**, 878 (2019).
- ¹⁶ M. Brandenbourger, X. Locsin, E. Lerner, and C. Coulais, *Nat. Commun.* **10**, 4608 (2019).
- ¹⁷ M. Sakhdari, M. Hajizadegan, Q. Zhong, D. N. Christodoulides, R. El-Ganainy, and P.-Y. Chen, *Phys. Rev. Lett.* **123**, 193901 (2019).
- ¹⁸ A. Tuniz, T. Wieduwilt, and M. A. Schmidt, *Phys. Rev. Lett.* **123**, 213903 (2019).
- ¹⁹ L. Xiao, K. Wang, X. Zhan, Z. Bian, K. Kawabata, M. Ueda, W. Yi, and P. Xue, *Phys. Rev. Lett.* **123**, 230401 (2019).
- ²⁰ M. V. Berry, *Czech. J. Phys.* **54**, 1039 (2004).
- ²¹ W. Heiss, *J. Phys. A* **45**, 444016 (2012).
- ²² C. Dembowski, H.-D. Gräf, H. L. Harney, A. Heine, W. D. Heiss, H. Rehfeld, and A. Richter, *Phys. Rev. Lett.* **86**, 787 (2001).
- ²³ B. Zhen, C. W. Hsu, Y. Igarashi, L. Lu, I. Kaminer, A. Pick, S.-L. Chua, J. D. Joannopoulos, and M. Soljačić, *Nature (London)* **525**, 354 (2015).
- ²⁴ K. Ding, G. Ma, M. Xiao, Z. Q. Zhang, and C. T. Chan, *Phys. Rev. X* **6**, 021007 (2016).
- ²⁵ H. Zhou, C. Peng, Y. Yoon, C. W. Hsu, K. A. Nelson, L. Fu, J. D. Joannopoulos, M. Soljačić, and B. Zhen, *Science* **359**, 1009 (2018).
- ²⁶ K. Ding, G. Ma, Z. Q. Zhang, and C. T. Chan, *Phys. Rev. Lett.* **121**, 085702 (2018).
- ²⁷ A. Cerjan, S. Huang, M. Wang, K. P. Chen, Y. Chong, and M. C. Rechtsman, *Nat. Photonics*, 1 (2019).
- ²⁸ X. Zhang, K. Ding, X. Zhou, J. Xu, and D. Jin, *Phys. Rev. Lett.* **123**, 237202 (2019).
- ²⁹ A. Guo, G. J. Salamo, D. Duchesne, R. Morandotti, M. Volatier-Ravat, V. Aimez, G. A. Siviloglou, and D. N. Christodoulides, *Phys. Rev. Lett.* **103**, 093902 (2009).
- ³⁰ L. Feng, Y.-L. Xu, W. S. Fegadolli, M.-H. Lu, J. E. Oliveira, V. R. Almeida, Y.-F. Chen, and A. Scherer, *Nat. Mater.* **12**, 108 (2013).
- ³¹ M. Brandstetter, M. Liertzer, C. Deutsch, P. Klang, J. Schöberl, H. Türeci, G. Strasser, K. Unterrainer, and S. Rotter, *Nat. Commun.* **5**, 4034 (2014).
- ³² W. Chen, Ş. K. Özdemir, G. Zhao, J. Wiersig, and L. Yang, *Nature (London)* **548**, 192 (2017).
- ³³ X. Wang, X. Fang, D. Mao, Y. Jing, and Y. Li, *Phys. Rev. Lett.* **123**, 214302 (2019).
- ³⁴ K. Ding, Z. Q. Zhang, and C. T. Chan, *Phys. Rev. B* **92**, 235310 (2015).
- ³⁵ T. E. Lee, *Phys. Rev. Lett.* **116**, 133903 (2016).
- ³⁶ Z. Lin, A. Pick, M. Lončar, and A. W. Rodriguez, *Phys. Rev. Lett.* **117**, 107402 (2016).
- ³⁷ D. Leykam, K. Y. Bliokh, C. Huang, Y. D. Chong, and F. Nori, *Phys. Rev. Lett.* **118**, 040401 (2017).
- ³⁸ Y. Xu, S.-T. Wang, and L.-M. Duan, *Phys. Rev. Lett.* **118**, 045701 (2017).
- ³⁹ J. González and R. A. Molina, *Phys. Rev. B* **96**, 045437 (2017).
- ⁴⁰ A. A. Zyuzin and A. Y. Zyuzin, *Phys. Rev. B* **97**, 041203(R) (2018).
- ⁴¹ J. Wang, H. Y. Dong, Q. Y. Shi, W. Wang, and K. H. Fung, *Phys. Rev. B* **97**, 014428 (2018).
- ⁴² V. M. Martinez Alvarez, J. E. Barrios Vargas, and L. E. F. Foa Torres, *Phys. Rev. B* **97**, 121401(R) (2018).
- ⁴³ R. A. Molina and J. González, *Phys. Rev. Lett.* **120**, 146601 (2018).
- ⁴⁴ L. Jin and Z. Song, *Phys. Rev. Lett.* **121**, 073901 (2018).
- ⁴⁵ J. Carlström and E. J. Bergholtz, *Phys. Rev. A* **98**, 042114 (2018).
- ⁴⁶ L. Pan, S. Chen, and X. Cui, *Phys. Rev. A* **99**, 011601(R) (2019).
- ⁴⁷ K. Moors, A. A. Zyuzin, A. Y. Zyuzin, R. P. Tiwari, and T. L. Schmidt, *Phys. Rev. B* **99**, 041116(R) (2019).
- ⁴⁸ J. C. Budich, J. Carlström, F. K. Kunst, and E. J. Bergholtz, *Phys. Rev. B* **99**, 041406(R) (2019).
- ⁴⁹ Z. Yang and J. Hu, *Phys. Rev. B* **99**, 081102(R) (2019).
- ⁵⁰ H. Zhou, J. Y. Lee, S. Liu, and B. Zhen, *Optica* **6**, 190 (2019).
- ⁵¹ B. Zhu, Q. J. Wang, and Y. D. Chong, *Phys. Rev. A* **99**, 033829 (2019).
- ⁵² N. Hatano, *Mol. Phys.* **117**, 2121 (2019).
- ⁵³ S. Chen, W. Zhang, B. Yang, T. Wu, and X. Zhang, *Sci. Rep.* **9**, 5551 (2019).
- ⁵⁴ K. L. Zhang, P. Wang, and Z. Song, *Phys. Rev. A* **99**, 042111 (2019).
- ⁵⁵ Q. Zhong, J. Ren, M. Khajavikhan, D. N. Christodoulides, i. m. c. K. Özdemir, and R. El-Ganainy, *Phys. Rev. Lett.* **122**, 153902 (2019).
- ⁵⁶ J. Carlström, M. Stålhammar, J. C. Budich, and E. J. Bergholtz, *Phys. Rev. B* **99**, 161115 (2019).
- ⁵⁷ A. A. Zyuzin and P. Simon, *Phys. Rev. B* **99**, 165145 (2019).
- ⁵⁸ Y.-X. Xiao, Z.-Q. Zhang, Z. H. Hang, and C. T. Chan, *Phys. Rev. B* **99**, 241403(R) (2019).
- ⁵⁹ L. Pan, S. Chen, and X. Cui, *Phys. Rev. A* **99**, 063616 (2019).
- ⁶⁰ W. B. Rui, Y. X. Zhao, and A. P. Schnyder, *Phys. Rev. B* **99**, 241110 (2019).
- ⁶¹ K. Kimura, T. Yoshida, and N. Kawakami, *Phys. Rev. B* **100**, 115124 (2019).
- ⁶² R. Okugawa and T. Yokoyama, *Phys. Rev. B* **99**, 041202(R) (2019).
- ⁶³ K. Kawabata, T. Bessho, and M. Sato, *Phys. Rev. Lett.* **123**, 066405 (2019).
- ⁶⁴ T. Yoshida, R. Peters, N. Kawakami, and Y. Hatsugai, *Phys. Rev. B* **99**, 121101(R) (2019).
- ⁶⁵ S. Lin, L. Jin, and Z. Song, *Phys. Rev. B* **99**, 165148 (2019).
- ⁶⁶ T. Yoshida and Y. Hatsugai, *Phys. Rev. B* **100**, 054109 (2019).
- ⁶⁷ M. S. Rudner and L. S. Levitov, *Phys. Rev. Lett.* **102**, 065703 (2009).
- ⁶⁸ Y. C. Hu and T. L. Hughes, *Phys. Rev. B* **84**, 153101 (2011).
- ⁶⁹ K. Esaki, M. Sato, K. Hasebe, and M. Kohmoto,

- Phys. Rev. B **84**, 205128 (2011).
- ⁷⁰ V. Kozii and L. Fu, arXiv:1708.05841.
- ⁷¹ G. Harari, M. A. Bandres, Y. Lumer, M. C. Rechtsman, Y. D. Chong, M. Khajavikhan, D. N. Christodoulides, and M. Segev, *Science* **359**, eaar4003 (2018).
- ⁷² H. Shen, B. Zhen, and L. Fu, *Phys. Rev. Lett.* **120**, 146402 (2018).
- ⁷³ T. Yoshida, R. Peters, and N. Kawakami, *Phys. Rev. B* **98**, 035141 (2018).
- ⁷⁴ Z. Gong, Y. Ashida, K. Kawabata, K. Takasan, S. Higashikawa, and M. Ueda, *Phys. Rev. X* **8**, 031079 (2018).
- ⁷⁵ T. M. Philip, M. R. Hirsbrunner, and M. J. Gilbert, *Phys. Rev. B* **98**, 155430 (2018).
- ⁷⁶ Y. Chen and H. Zhai, *Phys. Rev. B* **98**, 245130 (2018).
- ⁷⁷ C.-H. Liu, H. Jiang, and S. Chen, *Phys. Rev. B* **99**, 125103 (2019).
- ⁷⁸ M. Papaj, H. Isobe, and L. Fu, *Phys. Rev. B* **99**, 201107 (2019).
- ⁷⁹ P. A. McClarty and J. G. Rau, *Phys. Rev. B* **100**, 100405(R) (2019).
- ⁸⁰ Y. Xiong, *J. Phys. Commun.* **2**, 035043 (2018).
- ⁸¹ C. Yin, H. Jiang, L. Li, R. Lü, and S. Chen, *Phys. Rev. A* **97**, 052115 (2018).
- ⁸² F. K. Kunst, E. Edvardsson, J. C. Budich, and E. J. Bergholtz, *Phys. Rev. Lett.* **121**, 026808 (2018).
- ⁸³ S. Yao and Z. Wang, *Phys. Rev. Lett.* **121**, 086803 (2018).
- ⁸⁴ S. Malzard and H. Schomerus, *Phys. Rev. A* **98**, 033807 (2018).
- ⁸⁵ S. Yao, F. Song, and Z. Wang, *Phys. Rev. Lett.* **121**, 136802 (2018).
- ⁸⁶ K. Kawabata, K. Shiozaki, and M. Ueda, *Phys. Rev. B* **98**, 165148 (2018).
- ⁸⁷ K. Takata and M. Notomi, *Phys. Rev. Lett.* **121**, 213902 (2018).
- ⁸⁸ C. Yuce and Z. Oztas, *Sci. Rep.* **8**, 17416 (2018).
- ⁸⁹ K. Kawabata, S. Higashikawa, Z. Gong, Y. Ashida, and M. Ueda, *Nat. Commun.* **10**, 297 (2019).
- ⁹⁰ L. Jin and Z. Song, *Phys. Rev. B* **99**, 081103(R) (2019).
- ⁹¹ K. Y. Bliokh, D. Leykam, M. Lein, and F. Nori, *Nat. Commun.* **10**, 580 (2019).
- ⁹² H. Wang, J. Ruan, and H. Zhang, *Phys. Rev. B* **99**, 075130 (2019).
- ⁹³ T. Liu, Y.-R. Zhang, Q. Ai, Z. Gong, K. Kawabata, M. Ueda, and F. Nori, *Phys. Rev. Lett.* **122**, 076801 (2019).
- ⁹⁴ E. Edvardsson, F. K. Kunst, and E. J. Bergholtz, *Phys. Rev. B* **99**, 081302(R) (2019).
- ⁹⁵ C. H. Lee and R. Thomale, *Phys. Rev. B* **99**, 201103(R) (2019).
- ⁹⁶ L. Herviou, J. H. Bardarson, and N. Regnault, *Phys. Rev. A* **99**, 052118 (2019).
- ⁹⁷ F. K. Kunst and V. Dwivedi, *Phys. Rev. B* **99**, 245116 (2019).
- ⁹⁸ T.-S. Deng and W. Yi, *Phys. Rev. B* **100**, 035102 (2019).
- ⁹⁹ M. Ezawa, *Phys. Rev. B* **100**, 045407 (2019).
- ¹⁰⁰ K. L. Zhang, H. C. Wu, L. Jin, and Z. Song, *Phys. Rev. B* **100**, 045141 (2019).
- ¹⁰¹ L. Li, C. H. Lee, and J. Gong, *Phys. Rev. B* **100**, 075403 (2019).
- ¹⁰² K. Yokomizo and S. Murakami, *Phys. Rev. Lett.* **123**, 066404 (2019).
- ¹⁰³ Z.-Y. Ge, Y.-R. Zhang, T. Liu, S.-W. Li, H. Fan, and F. Nori, *Phys. Rev. B* **100**, 054105 (2019).
- ¹⁰⁴ N. Okuma and M. Sato, *Phys. Rev. Lett.* **123**, 097701 (2019).
- ¹⁰⁵ S. Longhi, *Phys. Rev. Research* **1**, 023013 (2019).
- ¹⁰⁶ K. Zhang, Z. Yang, and C. Fang, arXiv:1910.01131.
- ¹⁰⁷ N. Okuma, K. Kawabata, K. Shiozaki, and M. Sato, arXiv:1910.02878.
- ¹⁰⁸ H. C. Wu, L. Jin, and Z. Song, *Phys. Rev. B* **100**, 155117 (2019).
- ¹⁰⁹ W. Brzezicki and T. Hyart, *Phys. Rev. B* **100**, 161105(R) (2019).
- ¹¹⁰ K. Kawabata, K. Shiozaki, M. Ueda, and M. Sato, *Phys. Rev. X* **9**, 041015 (2019).
- ¹¹¹ P. San-Jose, J. Cayao, E. Prada, and R. Aguado, *Sci. Rep.* **6**, 21427 (2016).
- ¹¹² C. Yuce, *Phys. Rev. A* **93**, 062130 (2016).
- ¹¹³ Q.-B. Zeng, B. Zhu, S. Chen, L. You, and R. Lü, *Phys. Rev. A* **94**, 022119 (2016).
- ¹¹⁴ H. Menke and M. M. Hirschmann, *Phys. Rev. B* **95**, 174506 (2017).
- ¹¹⁵ M. Klett, H. Cartarius, D. Dast, J. Main, and G. Wunner, *Phys. Rev. A* **95**, 053626 (2017).
- ¹¹⁶ C. Li, X. Z. Zhang, G. Zhang, and Z. Song, *Phys. Rev. B* **97**, 115436 (2018).
- ¹¹⁷ K. Kawabata, Y. Ashida, H. Katsura, and M. Ueda, *Phys. Rev. B* **98**, 085116 (2018).
- ¹¹⁸ M. van Caspel, S. E. T. Arze, and I. P. Castillo, *SciPost Phys.* **6**, 26 (2019).
- ¹¹⁹ S. Lieu, *Phys. Rev. B* **100**, 085110 (2019).
- ¹²⁰ A. Y. Kitaev, *Physics-Uspekhi* **44**, 131 (2001).
- ¹²¹ Z. Yang, K. Zhang, C. Fang, and J. Hu, arXiv:1912.05499.
- ¹²² See Supplemental Material.

Supplemental Material for “Topological semimetal phase with exceptional points in 1D non-Hermitian systems”

Kazuki Yokomizo¹ and Shuichi Murakami^{1,2}

¹*Department of Physics, Tokyo Institute of Technology,
2-12-1 Ookayama, Meguro-ku, Tokyo, 152-8551, Japan*

²*TIES, Tokyo Institute of Technology, 2-12-1 Ookayama, Meguro-ku, Tokyo, 152-8551, Japan*

SI. MOTION OF THE EXCEPTIONAL POINTS AND CHANGE OF THE VALUE OF THE WINDING NUMBER

In this section, we show that in one-dimensional (1D) non-Hermitian systems with both sublattice symmetry (SLS) and time-reversal symmetry (TRS), the value of the winding number changes through the creation and annihilation of the exceptional points as shown in Fig. S1. Here, for a real-space Hamiltonian H , the SLS and the TRS are defined as

$$\Gamma H \Gamma^{-1} = -H, \quad \mathcal{T} H^* \mathcal{T}^{-1} = H, \quad (\text{S1})$$

where Γ and \mathcal{T} are unitary matrices representing the SLS and the TRS, respectively.

A. General cases

First of all, we focus on a two-band model. Due to the SLS, we can write down the Bloch Hamiltonian $\mathcal{H}(\beta)$ of this system as

$$\mathcal{H}(\beta) = \begin{pmatrix} 0 & R_+(\beta) \\ R_-(\beta) & 0 \end{pmatrix}, \quad (\text{S2})$$

where $\beta \equiv e^{ik}$, $k \in \mathbb{C}$, and $R_{\pm}(\beta)$ are holomorphic functions for β . In the following, without loss of generality, we can write these functions as

$$R_{\pm}(\beta) = \frac{C_{\pm}}{\beta^{2m}} \prod_{i=1}^{2m} (\beta - \beta_i^{\pm}), \quad (\text{S3})$$

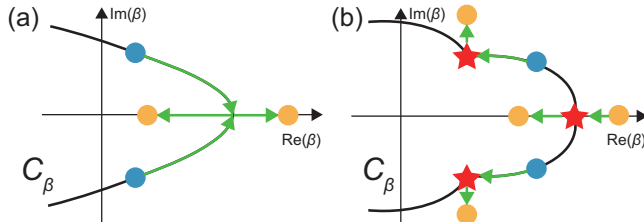


FIG. S1. Schematic figure of (a) coalescence of the exceptional points and (b) annihilation of the exceptional point at the cusp, respectively. The yellow (or blue) dots express the gap-closing points (or the exceptional points), and the red stars are the cusps of the generalized Brillouin zone C_{β} .

where C_{\pm} are real constants due to the TRS. Then the eigenvalue equation $\det[\mathcal{H}(\beta) - E] = R_+(\beta)R_-(\beta) - E^2 = 0$ can be explicitly written as

$$\frac{C_+ C_-}{\beta^{2m}} \prod_{i=1}^{2m} (\beta - \beta_i^+) (\beta - \beta_i^-) = E^2, \quad (\text{S4})$$

which is an algebraic equation for β with a degree $4m$. Here, by numbering the solutions of Eq. (S4) so as to satisfy $|\beta_1| \leq \dots \leq |\beta_{2M}|$, the condition for continuum bands¹ is given by

$$|\beta_M| = |\beta_{M+1}|, \quad (\text{S5})$$

and one can get the generalized Brillouin zone (GBZ) C_{β} from the trajectories of β_M and β_{M+1} . We note that C_{β} always encircles the origin on the complex plane^{2,3}.

In this case, this system is classified in terms of a Z topological invariant called winding number w , and it can be defined as¹

$$w = -\frac{w_+ - w_-}{2}, \quad w_{\pm} = \frac{1}{2\pi} [\arg R_{\pm}(\beta)]_{C_{\beta}}, \quad (\text{S6})$$

where $[\arg R_{\pm}(\beta)]_{C_{\beta}}$ means the change of the phase of the functions $R_{\pm}(\beta)$ as β goes along C_{β} in a counter-clockwise way. We note that as long as there is a gap at $E = 0$, $R_{\pm}(\beta)$ never vanish along C_{β} , and w is well defined. On the other hand, when the gap closes at $E = 0$, the gap-closing condition can be decoupled into two equations $R_+(\beta) = 0$ and $R_-(\beta) = 0$ being satisfied somewhere on C_{β} . At such a point, the Bloch Hamiltonian (S2) cannot be diagonalizable, and such point is called exceptional point. In this case, w is not well defined.

From Eq. (S3), we can rewrite this form as

$$w = -\frac{N_{\text{zeros}}^+ - N_{\text{zeros}}^-}{2}, \quad (\text{S7})$$

where N_{zeros}^{\pm} expresses the number of the solutions β_i^{\pm} of $R_{\pm}(\beta) = 0$ inside C_{β} , respectively. Furthermore it is worth noting that from Ref. 2, when the system has a gap around $E = 0$, we can get

$$\frac{1}{2\pi} \int_{C_{\beta}} d \log \det \mathcal{H}(\beta) = N_{\text{zeros}} - M = 0, \quad (\text{S8})$$

where $N_{\text{zeros}} (= N_{\text{zero}}^+ + N_{\text{zero}}^-)$ expresses the number of solutions of the equation $\det \mathcal{H}(\beta) = 0$ inside C_{β} . Equation (S8) tells us that the total number of the solutions

of $\det \mathcal{H}(\beta) = 0$ inside C_β , namely the number of the gap-closing points inside C_β , is unchanged as long as the system has a gap.

Now we focus on two insulator phases separated by the topological semimetal (TSM) phase with exceptional points. When the system enters the TSM phase from one of the insulator phases, the exceptional points are created by the inverse process as shown in Fig. S1(a) or (b). Then, after a further change of the system parameters, the system becomes the other insulator phase from the TSM phase, and here, the exceptional points are annihilated by the process as shown in Fig. S1(a) or (b). If the creation is by the inverse process of Fig. S1(a) and the annihilation is by the process of Fig. S1(b) (or vice versa), while the total number $N_{\text{zeros}} (= N_{\text{zero}}^+ + N_{\text{zero}}^-)$ of the solutions of $\det \mathcal{H}(\beta) = 0$ inside C_β is unchanged, such a motion of the exceptional points change the value of N_{zeros}^+ and N_{zeros}^- by 1 and -1 (or by -1 and 1), respectively, resulting in the change of w by 1 (or by -1). Therefore we conclude that these insulator phases have different values of w . We note that this scenario can be extended to multi-band systems.

B. Non-Hermitian Kitaev chain

We show an example of the non-Hermitian Kitaev chain with the SLS and TRS introduced in Eq. (4) in the main text. This model has the Bloch Hamiltonian $\mathcal{H}(\beta)$ as

$$\mathcal{H}(\beta) = \begin{pmatrix} 0 & R_+(\beta) \\ R_-(\beta) & 0 \end{pmatrix}, \quad (\text{S9})$$

where

$$R_\pm(\beta) = (t_b \pm \Delta_b) - \mu + (t_f \mp \Delta_f) \beta^{-1}, \quad (\text{S10})$$

and all the parameters are real. We note that the gap closes at $E = 0$ due to the SLS when either of the two quantities $R_\pm(\beta)$ is zero. We show the phase diagram of this model in Fig. S2(a) and its GBZ C_β , the solutions of the equations $R_\pm(\beta) = 0$, and the motion of the exceptional points in Fig. S2(c)-(h).

In the topological phase transition along the black arrow in Fig. S2(a), we show the position of the solutions β_1^+ and β_2^+ of $R_+(\beta) = 0$ (and β_1^- and β_2^- of $R_-(\beta) = 0$) as the red (and blue) dots and squares, respectively, as shown in Figs. S2(c-1)-(h-1). When we decrease the value of the parameter μ , at $\mu = 2.683$ (Fig. S2(g-1)), β_1^+ and β_2^+ change from real values to complex values via coalescence, and it corresponds to a pair creation of the exceptional points. After the coalescence, β_1^+ and β_2^+ become complex, with $\beta_1^+ = (\beta_2^+)^*$, and their common absolute value is between the values of $|\beta_1^-|$ and $|\beta_2^-|$, meaning that β_1^+ and β_2^+ stay on C_β . Then, at $\mu = 0.5813$ (Fig. S2(d-1)), the value of $|\beta_2^-|$ becomes equal to that of $|\beta_1^+|$ ($= |\beta_2^+|$), and after passing that point (i.e., μ becomes less than 0.5813), $|\beta_1^-| < |\beta_2^-| < |\beta_1^+| = |\beta_2^+|$,

meaning that β_1^+ and β_2^+ are no longer on C_β , and the gap opens (Fig. S2(c-1)). At the phase transition point $\mu = 0.5813$ (Fig. S2(d-1)), three solutions $\beta_1^+, \beta_2^+, \beta_2^-$ share the same absolute value, and the gap closes at three points on C_β , and at such points, C_β has cusps.

The change of the winding number w defined as Eq. (S6) readily follows from the following argument. In the normal insulator (NI) phase with $w = 0$, C_β surrounds one solution of $R_+(\beta) = 0$ and one solution of $R_-(\beta) = 0$ (Fig. S2(h-1)). In this case, $w_\pm = [\arg R_\pm(\beta)]_{C_\beta} / 2\pi = 0$ because $R_\pm(\beta)$ is proportional to $(\beta - \beta_1^\pm)(\beta - \beta_2^\pm) / \beta$. On the other hand, in the topological insulator (TI) phase with $w = 1$, there exist two solutions of $R_-(\beta) = 0$ and no solutions of $R_+(\beta) = 0$ inside C_β (Fig. S2(c-1)), which leads to $w_- = 1$, $w_+ = -1$, and $w = 1$ as expected. Therefore the creation and annihilation of the exceptional points changes the number of the solutions of $R_\pm(\beta) = 0$ inside C_β , and the value of the topological invariant also changes.

We note that in addition to the topological phase transition between two insulator phases via the TSM phase, a direct phase transition from the NI phase to the TI phase is also possible as shown in the inset of Fig. S2(a). Here the gap closes on the real axis, where $R_+(\beta)$ and $R_-(\beta)$ simultaneously become zero at this value of β .

SIII. 1D NON-HERMITIAN SYSTEM WITH PSEUDO PARTICLE-HOLE SYMMETRY

In this section, we investigate a 1D non-Hermitian system with pseudo particle-hole symmetry (PHS) and show that it is classified in terms of a Z_2 topological invariant. Here, for a real-space Hamiltonian H , this symmetry is defined as

$$\mathcal{C}H^*\mathcal{C}^{-1} = -H, \quad (\text{S11})$$

where \mathcal{C} is the unitary matrix. In the following, we focus on a two-band model.

A. Two-band model

The Bloch Hamiltonian $\mathcal{H}(\beta)$ can be written as

$$\mathcal{H}(\beta) = \mathcal{H}_0(\beta) \sigma_0 + \sum_{i=x,y,z} \mathcal{H}_i(\beta) \sigma_i, \quad (\text{S12})$$

where σ_0 is a 2×2 identity matrix, σ_i ($i = x, y, z$) are the Pauli matrices, and the complex Bloch wave number is defined as $\beta \equiv e^{ik}$, $k \in \mathbb{C}$. We assume that it satisfies

$$\sigma_x [\mathcal{H}(\beta)]^* \sigma_x^{-1} = -\mathcal{H}(\beta^*), \quad (\text{S13})$$

and then, the coefficients $\mathcal{H}_i(\beta)$ ($i = 0, x, y, z$) in Eq. (S12) satisfy

$$[\mathcal{H}_i(\beta)]^* = -\mathcal{H}_i(\beta^*) \quad (i = 0, x, y), \quad [\mathcal{H}_z(\beta)]^* = \mathcal{H}_z(\beta^*). \quad (\text{S14})$$

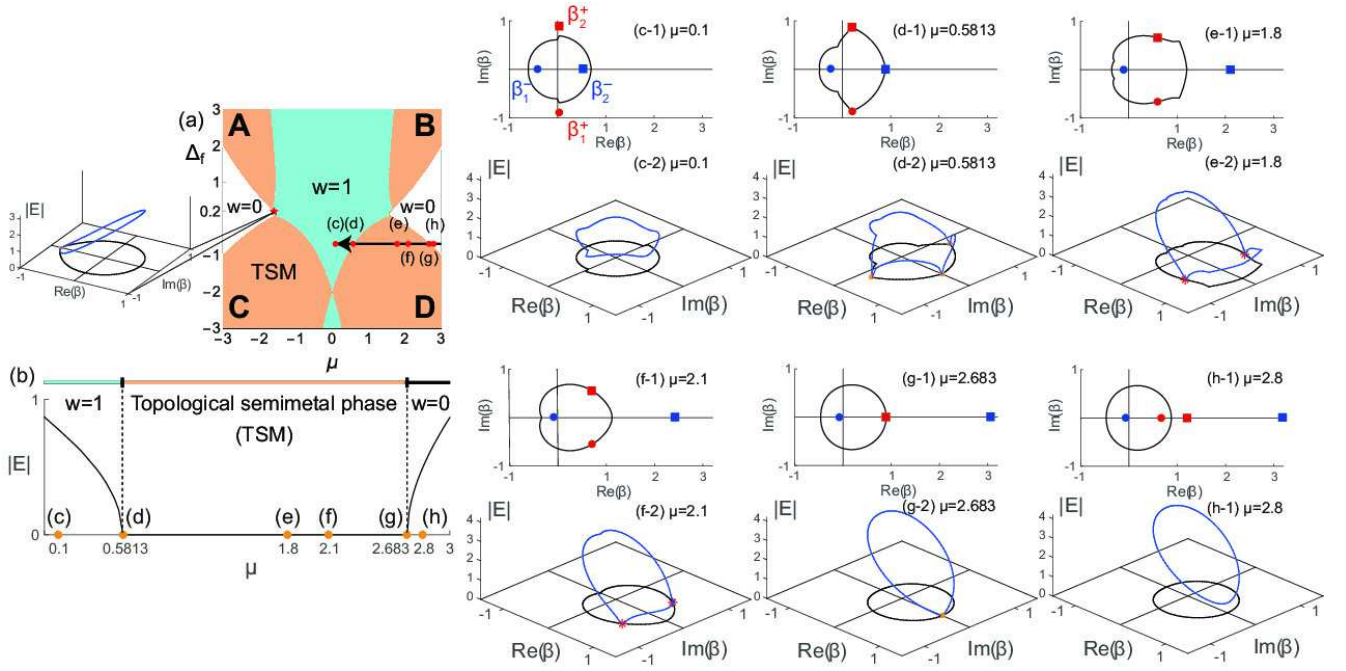


FIG. S2. (a) Phase diagram in the non-Hermitian Kitaev chain with $k \in \mathbb{C}$ with the values of the parameters to be $t_b = 1.2$, $t_f = 0.5$, $\Delta_b = 0.3$. At the red star ($\mu = -1.5922$ and $\Delta_f = 0.2$), the gap closes, and a direct transition between two insulator phases with $w = 0$ (white region) and $w = 1$ (blue region) occurs. The orange regions express topological semimetal (TSM) phase. (b) Continuum band along the black arrow ($\Delta_f = -0.7$) in (a). Since it is a two-band model with the sublattice symmetry, we only show $|E|$ to see whether the gap closes. (c)-(h) Solutions of the equations $R_{\pm}(\beta) = 0$, generalized Brillouin zone, and motion of the exceptional points along the black arrow in (a). The red (or blue) dots and squares express the solutions of $R_+(\beta) = 0$ (or $R_-(\beta) = 0$).

It is worth noting that $\mathcal{H}_i(\beta)$ ($i = 0, x, y$) are a pure imaginary and $\mathcal{H}_z(\beta)$ is real when $\arg \beta = 0$ and $\arg \beta = \pi$.

B. Z_2 topological invariant

Such a system is classified in terms of the Z_2 topological invariant ν ($= 0, 1$), and for the Bloch Hamiltonian (S12), we can define it as

$$\nu = \frac{1}{2\pi} \int_{\beta_0}^{\beta_\pi} d\beta \frac{d}{d\beta} [\arg \mathcal{R}_+(\beta) - \arg \mathcal{R}_-(\beta)] \pmod{2},$$

$$\mathcal{R}_{\pm}(\beta) = \mathcal{H}_z(\beta) \pm i\sqrt{\mathcal{H}_x^2(\beta) + \mathcal{H}_y^2(\beta)}, \quad (\text{S15})$$

where β_0 (or β_π) is the value of β at $\arg \beta = 0$ (or $\arg \beta = \pi$) on the GBZ C_β (for example, see Fig. S3). In Eq. (S15), the integral contour β goes along C_β , and we select the branch cut of the square root so that the both functions $\mathcal{R}_{\pm}(\beta)$ becomes continuous on C_β .

In the following, we assume that a system has a gap. Here we note that two continuum bands are separated by a line which determines a complex gap on the complex energy plane. This gap is called a line gap⁵. In this case, one can show that ν takes only 0 or 1. To this end, we calculate the value of $\exp(2\pi i\nu)$. As mentioned in

Sec. SII A, since the functions $\mathcal{R}_{\pm}(\beta_0)$ and $\mathcal{R}_{\pm}(\beta_\pi)$ take real values, we can rewrite the expression of $\exp(2\pi i\nu)$ as

$$\begin{aligned} \exp(2\pi i\nu) &= \exp\{i[\arg \mathcal{R}_+(\beta_\pi) - \arg \mathcal{R}_+(\beta_0)]\} \\ &\quad \times \exp\{i[\arg \mathcal{R}_-(\beta_\pi) - \arg \mathcal{R}_-(\beta_0)]\} \\ &= \frac{\text{sgn}[\mathcal{R}_+(\beta_\pi)] \text{sgn}[\mathcal{R}_-(\beta_\pi)]}{\text{sgn}[\mathcal{R}_+(\beta_0)] \text{sgn}[\mathcal{R}_-(\beta_0)]} \\ &= \prod_{\beta=\beta_0, \beta_\pi} \prod_{\sigma=\pm} \text{sgn}[\mathcal{R}_\sigma(\beta)] \\ &= \prod_{\beta=\beta_0, \beta_\pi} \text{sgn} \left[\sum_{i=x,y,z} \mathcal{H}_i^2(\beta) \right]. \end{aligned} \quad (\text{S16})$$

Here we note that the quantities $\sum_i \mathcal{H}_i^2(\beta_0)$ and $\sum_i \mathcal{H}_i^2(\beta_\pi)$ are real. Since we assume presence of a line gap, we conclude that $\sum_i \mathcal{H}_i^2(\beta_0)$ and $\sum_i \mathcal{H}_i^2(\beta_\pi)$ have the same sign, as we prove by contradiction in the following.

Suppose $\sum_i \mathcal{H}_i^2(\beta_0)$ and $\sum_i \mathcal{H}_i^2(\beta_\pi)$ have different signs. We can set

$$\sum_{i=x,y,z} \mathcal{H}_i^2(\beta_0) > 0, \quad \sum_{i=x,y,z} \mathcal{H}_i^2(\beta_\pi) < 0 \quad (\text{S17})$$

without loss of generality. First of all, we assume

$\mathcal{H}_0(\beta) = 0$ for simplicity. At $\beta = \beta_0$, the energies are $E = \pm\varepsilon_0$, $\varepsilon_0 = \sqrt{\sum_i \mathcal{H}_i^2(\beta_0)} > 0$. Now we choose $E = \varepsilon_0 = \sqrt{\sum_i \mathcal{H}_i^2(\beta_0)}$, and we change β along C_β in a counterclockwise way from $\beta = \beta_0$ to $\beta = \beta_\pi$. Here, let C_+ denote this path on the complex plane. Then, at $\beta = \beta_\pi$, the energy is given by $E = \varepsilon_\pi = \sqrt{\sum_i \mathcal{H}_i^2(\beta_\pi)} \in i\mathbb{R}$, where the branch of the square root is chosen in such a way that $E = \sqrt{\sum_i \mathcal{H}_i^2(\beta)}$ is continuous along C_+ . Next we consider a path C_- along C_β in a clockwise way from $\beta = \beta_0$ to $\beta = \beta_\pi$. Because $[\sum_i \mathcal{H}_i^2(\beta)]^* = [\sum_i \mathcal{H}_i^2(\beta^*)]$, the energy at β and that at β^* are complex conjugate. Therefore, because $(C_+)^* = C_-$, the energy at $\beta = \beta_\pi$ along C_- is $E = \varepsilon_\pi^* = -\varepsilon_\pi$. Thus, by encircling $C_\beta (= -C_- + C_+)$ once from β_π to β_π , the branch changes from $E = -\varepsilon_\pi$ to $E = \varepsilon_\pi$, meaning that the two energies $E = \pm\sqrt{\sum_i \mathcal{H}_i^2(\beta)}$ are continuously connected, and there is no line gap, contradicting the assumption. Thus we can conclude that $\sum_i \mathcal{H}_i^2(\beta_0)$ and $\sum_i \mathcal{H}_i^2(\beta_\pi)$ have the same sign. So far, we assume $\mathcal{H}_0(\beta) = 0$, but even in the case of $\mathcal{H}_0(\beta) \neq 0$, because this term does not affect above argument, the above proof remains valid.

Therefore, from Eq. (S16), we can get $\exp(2\pi i\nu) = 1$ and can conclude that the value of ν is an integer. As a result, ν can take only 0 or 1 (mod 2), and we conclude that ν can be interpreted as the Z_2 topological invariant in this system.

In particular, in Hermitian cases, we can greatly simplify the formula of ν in Eq. (S15). The Bloch wave number k becomes real, and the all coefficients included in Eq. (S12) become real functions. In the following, we replace $\mathcal{H}_i(\beta)$ by $H_i(k)$ ($i = 0, x, y, z$), $k \in [-\pi, \pi]$. Here the system has the conventional PHS represented as

$$H_i(k) = -H_i(-k) \quad (i = 0, x, y), \quad H_z(k) = H_z(-k), \quad (\text{S18})$$

and $H_i(k)$ ($i = 0, x, y$) become zero at $k = 0$ and $k = \pi$. Furthermore we can get

$$\arg\left(H_z - i\sqrt{H_x^2 + H_y^2}\right) = -\arg\left(H_z + i\sqrt{H_x^2 + H_y^2}\right), \quad (\text{S19})$$

and then, Eq. (S15) can be rewritten as

$$\begin{aligned} \nu &= \frac{1}{\pi} \int_0^\pi dk \frac{d}{dk} \arg\left[H_z(k) + i\sqrt{H_x^2(k) + H_y^2(k)}\right] \\ &= \frac{1}{\pi} [\arg H_z(k)]_0^\pi. \end{aligned} \quad (\text{S20})$$

Since Eq. (S18) tells us that both $\arg H_z(0)$ and $\arg H_z(\pi)$ take 0 or π (mod 2π), Eq. (S20) can be further rewritten as

$$\nu = \begin{cases} 0 & \text{if } \text{sgn}[H_z(0)] \text{sgn}[H_z(\pi)] > 0, \\ 1 & \text{if } \text{sgn}[H_z(0)] \text{sgn}[H_z(\pi)] < 0, \end{cases} \quad (\text{S21})$$

and we obtain the known formula⁶

$$(-1)^\nu = \text{sgn}[H_z(0)] \text{sgn}[H_z(\pi)]. \quad (\text{S22})$$

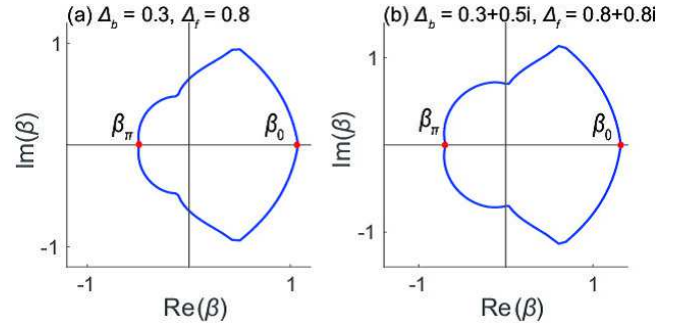


FIG. S3. Generalized Brillouin zone C_β in the generalized non-Hermitian Kitaev chain. The values of the parameters are $\gamma = 0$, $t_b = 1.2$, $t_f = 0.5$, and $\mu = 1$; (a) $\Delta_b = 0.3$ and $\Delta_f = 0.8$, and (b) $\Delta_b = 0.3 + 0.5i$ and $\Delta_f = 0.8 + 0.8i$. The points where C_β intersects the positive and negative sides of a real axis are denoted by β_0 and β_π , respectively.

C. Generalized non-Hermitian Kitaev chain

In this subsection, we study the generalized non-Hermitian Kitaev chain⁴. This system has the pseudo PHS, and as we discussed previously, it can be classified in terms of the Z_2 topological invariant ν defined in Eq. (S15). The real-space Hamiltonian of this system can be written as

$$\begin{aligned} H &= \sum_n \left[t_b c_n^\dagger c_{n+1} - t_b^* c_n c_{n+1}^\dagger + t_f c_{n+1}^\dagger c_n - t_f^* c_{n+1} c_n^\dagger \right. \\ &\quad \left. - i\Delta_b c_n^\dagger c_{n+1}^\dagger - i\Delta_b^* c_n c_{n+1} + i\Delta_f c_{n+1}^\dagger c_n^\dagger + i\Delta_f^* c_{n+1} c_n \right. \\ &\quad \left. + (i\gamma - \mu) c_n^\dagger c_n + (i\gamma + \mu) c_n c_n^\dagger \right], \end{aligned} \quad (\text{S23})$$

where γ represents dissipation, t_b and t_f are asymmetric hopping amplitudes, Δ_b and Δ_f are imbalanced pairing amplitudes, and μ is a chemical potential. γ and μ are real and, t_b, t_f, Δ_b , and Δ_f are complex. We note that this Hamiltonian reduces to that of the non-Hermitian Kitaev chain introduced in the main text when $\gamma = 0$, and $t_b, t_f, \Delta_b, \Delta_f \in \mathbb{R}$.

Here, for the Bloch Hamiltonian $\mathcal{H}(\beta)$ in the form (S12), the coefficients $\mathcal{H}_i(\beta)$ ($i = 0, x, y, z$) are given by

$$\begin{aligned} \mathcal{H}_0(\beta) &= i\gamma + i\Im(t_b)\beta + i\Im(t_f)\beta^{-1}, \\ \mathcal{H}_x(\beta) &= -i[\Re(\Delta_b)\beta - \Re(\Delta_f)\beta^{-1}], \\ \mathcal{H}_y(\beta) &= i[\Im(\Delta_b)\beta - \Im(\Delta_f)\beta^{-1}], \\ \mathcal{H}_z(\beta) &= \Re(t_b)\beta + \Re(t_f)\beta^{-1} - \mu. \end{aligned} \quad (\text{S24})$$

Then we can explicitly write the eigenvalue equation $\det[\mathcal{H}(\beta) - E] = 0$ as

$$\begin{aligned} &\left(|\Delta_b|^2 - |t_b|^2\right)\beta^2 + [2\mu\Re(t_b) - 2i(E - i\gamma)\Im(t_b)]\beta \\ &\quad - 2[\Re(\Delta_b\Delta_f^*) + \Re(t_b t_f^*)] + (E - i\gamma)^2 - \mu^2 \\ &\quad + [2\mu\Re(t_f) - 2i(E - i\gamma)\Im(t_f)]\beta^{-1} \\ &\quad + \left(|\Delta_f|^2 - |t_f|^2\right)\beta^{-2} = 0. \end{aligned} \quad (\text{S25})$$

Since Eq. (S25) is a quartic equation for β , the condition for continuum bands can be written as $|\beta_2| = |\beta_3|$ when the solutions of Eq. (S25) satisfy $|\beta_1| \leq |\beta_2| \leq |\beta_3| \leq |\beta_4|$. We note that the trajectories of β_2 and β_3 give the GBZ C_β . The examples of C_β and the continuum bands are given in Fig. S3 and in Fig. S4(a-3), respectively.

Let ℓ_\pm denote the loops drawn by the functions $\mathcal{R}_\pm(\beta)$ on the complex plane when β goes along C_β in a counter-clockwise way. Equation (S15) tells us how to determine the value of ν ; when neither ℓ_+ nor ℓ_- surrounds the origin \mathcal{O} on the complex plane, ν is equal to 0, and when two loops simultaneously surrounds \mathcal{O} , ν is equal to 1. For example, in the case of Fig. S4(a-4), ν becomes 1. We note that the system has the exceptional points when either ℓ_+ or ℓ_- passes \mathcal{O} , and ν is not well defined in this case.

We can get the phase diagram in the generalized non-Hermitian Kitaev chain as shown in Fig. S4(a) and can confirm that the topological edge states appear when ν takes the nonzero value as shown in Fig. S4(b). Therefore we can establish the bulk-edge correspondence between the Z_2 topological invariant ν and existence of the topological edge states.

In this model, we can see that the pseudo PHS cannot protect a TSM phase with exceptional points. For simplicity, let the parameter γ be zero. We note that by treating the parameters t_b and t_f as complex, one can add $\mathcal{H}_0(\beta)$ term to the Bloch Hamiltonian $\mathcal{H}(\beta)$ in the case of Fig. S4(a). In fact, for $\Im(t_b) = \Im(t_f) \neq 0$ being infinitesimal values as an example, we can obtain the phase diagram as shown in Fig. S4(b). We can confirm that the TSM phase with exceptional points in Fig. S4(a) disappears by adding $\mathcal{H}_0(\beta)$. We note that the exceptional points appear on the orange lines on the phase diagram. However, this exceptional point can be removed by adding other perturbation terms. Therefore we conclude that the pseudo PHS cannot protect the TSM phase with exceptional points.

III. RESTRICTION ON THE BLOCH WAVE NUMBER BY EITHER PARTICLE-HOLE SYMMETRY OR CHIRAL SYMMETRY

In this section, we show that in 1D non-Hermitian tight-binding systems, some symmetries make the Bloch wave number real even in an open chain. The previous work⁵ showed that it takes real values even in non-Hermitian cases under pseudo time-reversal symmetry (TRS) represented as

$$\mathcal{T}H^T\mathcal{T}^{-1} = H, \quad (\text{S26})$$

where H is a real-space Hamiltonian, and \mathcal{T} is a unitary matrix. Here we show that PHS or chiral symmetry (CS) also restricts the Bloch wave number to real values. In the following, we focus on a 1D real-space tight-binding

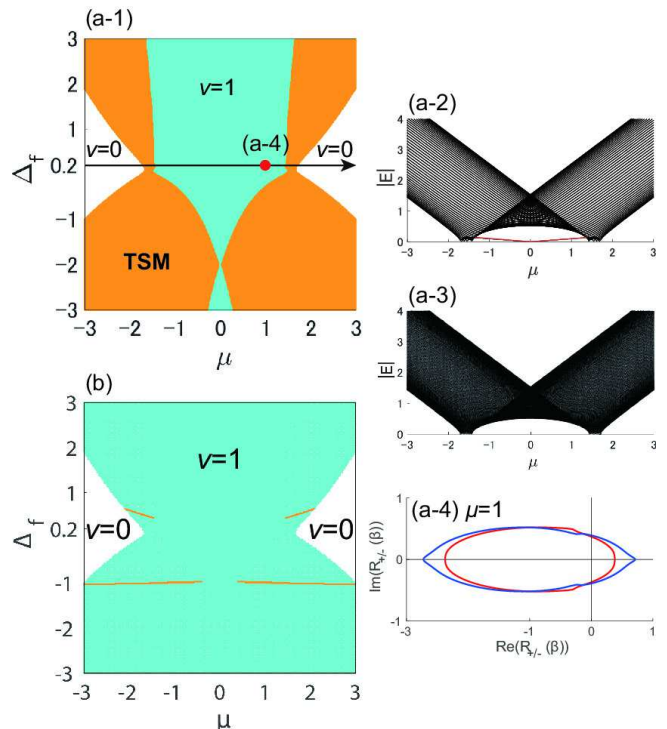


FIG. S4. (a) Phase diagram and bulk-edge correspondence in the generalized non-Hermitian Kitaev chain with $\gamma = 0$, $t_b = 1.2$, $t_f = 0.5$, and $\Delta_b = 0.3 + 0.2i$. We note that in this case, $\mathcal{H}_0(\beta) = 0$. We set the parameter Δ_f as real. (a-1) Phase diagram on the μ - Δ_f plane. The blue region represents a topological insulator phase with the Z_2 topological invariant ν equal to 1, the white region represents a normal insulator phase with $\nu = 0$, and the orange region represents a topological semimetal (TSM) phase with exceptional points. Along the black arrow in (a-1) with $\Delta_f = 0.2$, we show the results for (a-2) energy levels in a finite open chain and (a-3) the continuum bands. The edge states are shown in red in (a-2). (a-4) shows ℓ_+ (red) and ℓ_- (blue) on the \mathbf{R} plane with $\mu = 1$ and $\Delta_f = 0.2$. These loops encircle the origin on the complex plane, meaning that the value of ν is equal to 1. (b) Phase diagram in the generalized non-Hermitian Kitaev chain with $\mathcal{H}_0(\beta) \neq 0$. The parameters are set as $\Re(t_b) = 1.2$, $\Re(t_f) = 0.5$, $\Delta_b = 0.3 + 0.2i$, and $\Im(t_b) = \Im(t_f)$ takes infinitesimal values.

Hamiltonian

$$H = \sum_n \sum_{i=-N}^N \sum_{\mu, \nu=1}^q t_{i, \mu \nu} c_{n+i, \mu}^\dagger c_{n, \nu}, \quad (\text{S27})$$

where the unit cell is composed of q degrees of freedom, and the range of hopping is N . We note that this Hamiltonian can be non-Hermitian, meaning that $t_{i, \mu \nu}$ is not necessarily equal to $t_{-i, \nu \mu}^*$. Then a Bloch Hamiltonian $\mathcal{H}(\beta)$ is given by

$$[\mathcal{H}(\beta)]_{\mu \nu} = \sum_{i=-N}^N t_{i, \mu \nu} \beta^i, \quad (\mu, \nu = 1, \dots, q), \quad (\text{S28})$$

where the complex Bloch wave number is defined as $\beta = e^{ik}$, $k \in \mathbb{C}$. We assume that the eigenvalue equation $\det[\mathcal{H}(\beta) - E] = 0$ is an algebraic equation for β with an even degree $2M$, and $2M$ solutions of this equation satisfy $|\beta_1| \leq \dots \leq |\beta_{2M}|$. Here the condition for continuum bands is written as $|\beta_M| = |\beta_{M+1}|$, of which the detail is given in the main text and Ref. 1.

A. Particle-hole symmetry

The PHS⁵ is defined as

$$\mathcal{C}H^T\mathcal{C}^{-1} = -H, \quad (\text{S29})$$

where \mathcal{C} is unitary matrix. Here, for the real-space eigenvalue equation

$$H|\psi\rangle = E|\psi\rangle, \quad (\text{S30})$$

we can get

$$H(\mathcal{C}|\psi'\rangle) = -E(\mathcal{C}|\psi'\rangle) \quad (\text{S31})$$

due to the PHS. This is because the transposed matrix H^T has the same eigenvalues with H ; i.e., $H^T|\psi'\rangle = E|\psi'\rangle$. Because of Eq. (S31), the energy eigenvalues appear in pairs: $(E, -E)$. On the other hand, the hopping matrix $t_{i,\mu\nu}$ satisfies the condition

$$\sum_{\sigma,\tau=1}^q (\mathcal{C})_{\nu\sigma} t_{-i,\sigma\tau} (\mathcal{C}^{-1})_{\tau\mu} = -t_{i,\mu\nu} \quad (\text{S32})$$

due to the PHS. Then we can obtain the constraint for the Bloch Hamiltonian $\mathcal{H}(\beta)$ as

$$\mathcal{C}\mathcal{H}^T(\beta)\mathcal{C}^{-1} = -\mathcal{H}(\beta^{-1}), \quad (\text{S33})$$

and by using Eq. (S33), the eigenvalue equation $\det[\mathcal{H}(\beta) - E] = 0$ can be rewritten as

$$\det[\mathcal{H}(\beta^{-1}) + E] = 0. \quad (\text{S34})$$

On the other hand, $\det[\mathcal{H}(\beta) - E] = 0$ can be also rewritten as

$$\det[\mathcal{H}(\beta) + E] = 0. \quad (\text{S35})$$

because the energy eigenvalues appear in pairs: $(E, -E)$. By the combination of Eqs. (S34) and (S35), it is shown that the eigenvalue equation has the solutions in pairs: (β, β^{-1}) . Therefore the condition for continuum bands can be rewritten as

$$|\beta_M| = |\beta_{M+1}| = 1. \quad (\text{S36})$$

This represents that the Bloch wave number k takes real values because $|e^{ik}| = 1$ is satisfied.

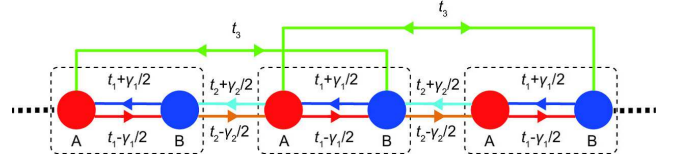


FIG. S5. Schematic figure of the non-Hermitian SSH model. The dotted boxes indicate the unit cell.

B. Chiral symmetry

The CS⁵ is defined as

$$\Gamma H^\dagger \Gamma^{-1} = -H, \quad (\text{S37})$$

where Γ is unitary matrix. Here, for the real-space eigenvalue equation

$$H|\psi\rangle = E|\psi\rangle, \quad (\text{S38})$$

we can get

$$H(\Gamma|\psi'\rangle) = -E^*(\Gamma|\psi'\rangle) \quad (\text{S39})$$

due to the CS. This is because the complex-conjugate transposed matrix H^\dagger has eigenvalues E^* ; i.e., $H^\dagger|\psi'\rangle = E^*|\psi'\rangle$. Because of Eq. (S39), the energy eigenvalues appear in pairs: $(E, -E^*)$. On the other hand, the hopping matrix $t_{i,\mu\nu}$ satisfies the condition

$$\sum_{\sigma,\tau=1}^q (\Gamma)_{\nu\sigma} t_{-i,\sigma\tau}^* (\Gamma^{-1})_{\tau\mu} = -t_{i,\mu\nu} \quad (\text{S40})$$

due to the CS. Then we can obtain the constraint for the Bloch Hamiltonian $\mathcal{H}(\beta)$ as

$$\Gamma\mathcal{H}^\dagger(\beta)\Gamma^{-1} = -\mathcal{H}(1/\beta^*), \quad (\text{S41})$$

and by using Eq. (S41), the eigenvalue equation $\det[\mathcal{H}(\beta) - E] = 0$ can be rewritten as

$$\det[\mathcal{H}(1/\beta^*) + E^*] = 0. \quad (\text{S42})$$

On the other hand, $\det[\mathcal{H}(\beta) - E] = 0$ can be also rewritten as

$$\det[\mathcal{H}(\beta) + E^*] = 0. \quad (\text{S43})$$

because the energy eigenvalues appear in pairs: $(E, -E^*)$. By the combination of Eqs. (S42) and (S43), it is shown that the eigenvalue equation has the solutions in pairs: $(\beta, 1/\beta^*)$. Therefore the condition for continuum bands also is given by Eq. (S36) in this case.

SIV. NON-HERMITIAN SSH MODEL

Our theory can apply to any 1D systems with both the SLS and the TRS. In this section, we investigate the TSM

phase with exceptional points in the non-Hermitian Su-Schrieffer-Heeger (SSH) model as shown in Fig. S5. We studied the topological phases and the bulk-edge correspondence in Ref. 1. The real-space Hamiltonian of this system is given by

$$H = \sum_n \left[\left(t_1 + \frac{\gamma_1}{2} \right) c_{n,A}^\dagger c_{n,B} + \left(t_1 - \frac{\gamma_1}{2} \right) c_{n,B}^\dagger c_{n,A} + \left(t_2 + \frac{\gamma_2}{2} \right) c_{n,B}^\dagger c_{n+1,A} + \left(t_2 - \frac{\gamma_2}{2} \right) c_{n+1,A}^\dagger c_{n,B} + t_3 \left(c_{n,A}^\dagger c_{n+1,B} + c_{n+1,B}^\dagger c_{n,A} \right) \right], \quad (\text{S44})$$

where t_1, t_2, t_3, γ_1 , and γ_2 are real. We note that this system has both the SLS and the TRS represented as Eq. (S1). The Bloch Hamiltonian $\mathcal{H}(\beta)$ can be obtained by a replacement $e^{ik} \rightarrow \beta$, similarly to Hermitian systems, as

$$\mathcal{H}(\beta) = \begin{pmatrix} 0 & R_+(\beta) \\ R_-(\beta) & 0 \end{pmatrix}, \quad (\text{S45})$$

where $R_\pm(\beta)$ are given by

$$R_+(\beta) = \left(t_2 - \frac{\gamma_2}{2} \right) \beta^{-1} + \left(t_1 + \frac{\gamma_1}{2} \right) + t_3 \beta, \\ R_-(\beta) = t_3 \beta^{-1} + \left(t_1 - \frac{\gamma_1}{2} \right) + \left(t_2 + \frac{\gamma_2}{2} \right) \beta, \quad (\text{S46})$$

respectively, and therefore, the eigenvalue equation can be written as

$$R_+(\beta) R_-(\beta) = E^2. \quad (\text{S47})$$

Here, since this system has the SLS, it can be characterized by the winding number w given by Eq. (S6).

Now we expect that the TSM phase with exceptional points is stable in the non-Hermitian SSH model. In fact, we can confirm that this TSM phase appears similarly to the non-Hermitian Kitaev chain with both the SLS and the TRS. In Fig. S6, we show the motion of the solutions of the equations $R_\pm(\beta) = 0$ as the system parameter γ_1 changes. When these points are on the GBZ C_β , the gap closes at $E = 0$. In this case, since either of two quantities $R_\pm(\beta)$ is zero somewhere on C_β , the solutions of either of $R_\pm(\beta) = 0$ express the exceptional points. As γ_1 changes between $\gamma_1 = 1.02$ and $\gamma_1 = 2.706$, C_β is deformed so that the exceptional points stay on C_β . Through the creation (at $\gamma_1 = 1.02$) and annihilation (at $\gamma_1 = 2.706$) of the exceptional points, the number of the solutions of $R_\pm(\beta) = 0$ inside C_β changes. Therefore the value of w also changes. In fact, while w becomes zero at $\gamma_1 = 2.8$ (Fig. S6(g)), it takes one at $\gamma_1 = 0.1$ (Fig. S6(b)).

¹ K. Yokomizo and S. Murakami, Phys. Rev. Lett. **123**, 066404 (2019).

² K. Zhang, Z. Yang, and C. Fang, arXiv:1910.01131.

³ Z. Yang, K. Zhang, C. Fang, and J. Hu, arXiv:1912.05499.

⁴ M. Ezawa, Phys. Rev. B **100**, 045407 (2019).

⁵ K. Kawabata, K. Shiozaki, M. Ueda, and M. Sato, Phys. Rev. X **9**, 041015 (2019).

⁶ A. Y. Kitaev, Physics-Uspekhi **44**, 131 (2001).

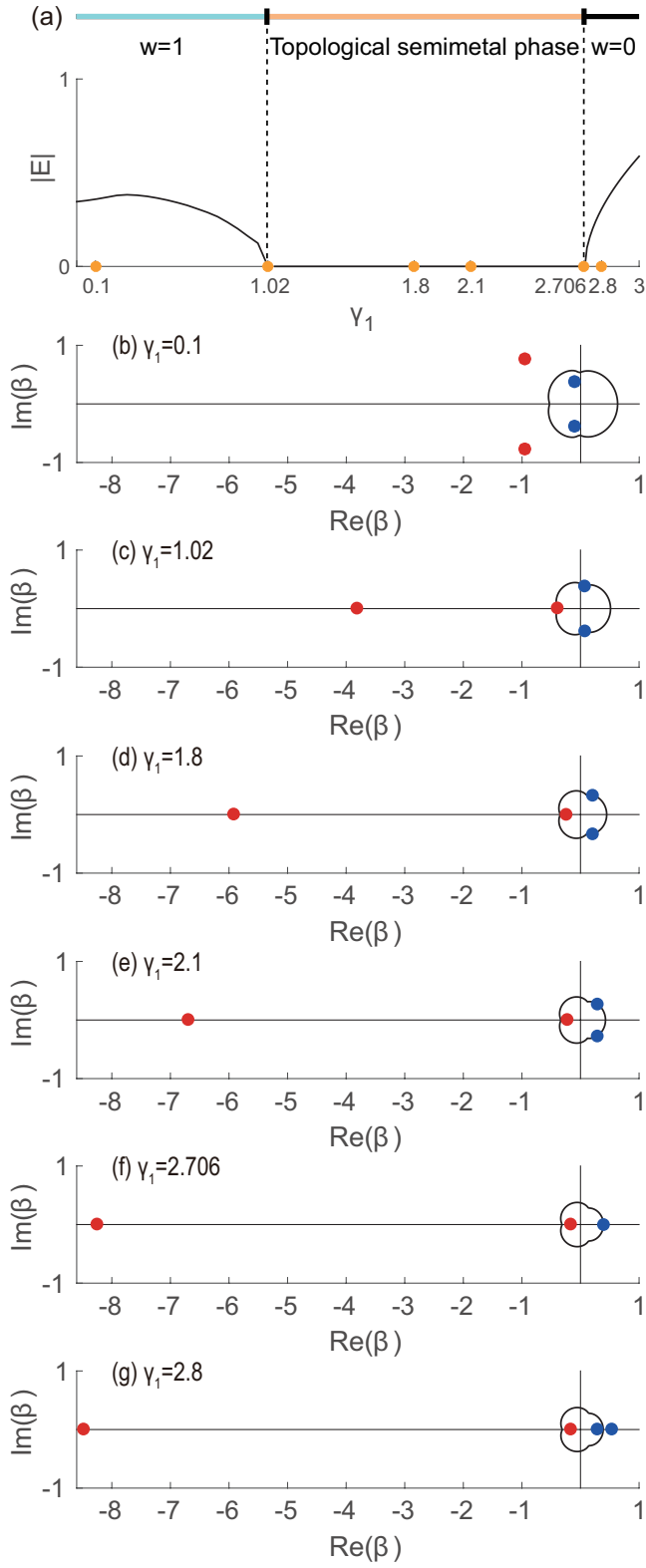


FIG. S6. (a) Phase diagram and continuum band in the non-Hermitian SSH model with the values of the parameters to be $t_1 = 1/3$, $t_2 = 0.8$, $t_3 = 1/5$, and $\gamma_2 = 1$ in an open chain. (b)-(g) Motions of the solutions of the eigenvalue equation (S47) for $E = 0$. The red dots express the solutions of the equation $R_+(\beta) = 0$, and the blue dots express those of $R_-(\beta) = 0$.